Temperature-Sensitive Random Insulin Granule Diffusion is a Prerequisite for Recruiting Granules for Release.

Ivarsson, Rosita; Obermüller, Stefanie; Rutter, Guy A; Galvanovskis, Juris; Renström, Erik

Published in:
Traffic: the International Journal of Intracellular Transport

DOI:
10.1111/j.1600-0854.2004.00216.x

2004

Traffic 2004; 5: 750–762
Blackwell Munksgaard

doi: 10.1111/j.1600-0854.2004.00216.x

Temperature-Sensitive Random Insulin Granule Diffusion is a Prerequisite for Recruiting Granules for Release

Rosita Ivarsson[1], Stefanie Obermüller[1], Guy A. Rutter[2], Juris Galvanovskis[1] and Erik Renström[1,*]

[1]The Diabetes Programme at Lund University, Department of Physiological Sciences, BMC B11, SE-221 84 Lund, Sweden
[2]Henry Wellcome Laboratories for Integrated Cell Signalling and Department of Biochemistry, University of Bristol, Bristol BS8 1TD, UK
** Corresponding author: Erik Renström, erik.renstrom@mphy.lu.se*

Glucose-evoked insulin secretion exhibits a biphasic time course and is associated with accelerated intracellular granule movement. We combined live confocal imaging of EGFP-labelled insulin granules with capacitance measurements of exocytosis in clonal INS-1 cells to explore the relation between distinct random and directed modes of insulin granule movement, as well as exocytotic capacity. Reducing the temperature from 34 °C to 24 °C caused a dramatic 81% drop in the frequency of directed events, but reduced directed velocities by a mere 25%. The much stronger temperature sensitivity of the frequency of directed events (estimated energy of activation ~ 135 kJ/mol) than that of the granule velocities (~ 22 kJ/mol) suggests that cooling-induced suppression of insulin granule movement is attributable to factors other than reduced motor protein adenosine 5′-triphosphatase activity. Indeed, cooling suppresses random granule diffusion by ~ 50%. In the single cell, the number of directed events depends on the extent of granule diffusion. Finally, single-cell exocytosis exhibits a biphasic pattern corresponding to that observed *in vivo*, and only the component reflecting 2nd phase insulin secretion is affected by cooling. We conclude that random diffusive movement is a prerequisite for directed insulin granule transport and for the recruitment of insulin granules released during 2nd phase insulin secretion.

Key words: diffusion, granule movement, insulin, microtubule, temperature sensitivity

Received 17 May 2004, revised and accepted for publication 23 June 2004

An increase in blood glucose stimulates insulin release in pancreatic β-cells via a chain of events that includes facilitated transport of the sugar into the cell, metabolic degradation by glycolysis and mitochondrial metabolism, resulting in an increased cytosolic adenosine 5′-triphosphatase/adenosine 5′-diphosphatase (ATP/ADP) ratio. The increase in ATP closes the ATP-sensitive K^+-channels with subsequent β-cell depolarization. The resultant depolarization leads to the activation of voltage-gated L-type $Ca_V1.2$ (1) and R-type $Ca_V2.3$ Ca^{2+} channels (2) and culminates in an increase in the cytoplasmic Ca^{2+} concentration that in turn triggers exocytosis of insulin granules (3). Glucose-evoked insulin secretion exhibits a characteristic biphasic release pattern, *in vivo* as well as in experimental systems (4,5). The rapid 1st phase typically lasts for up to 10 min and is followed by the less prominent but sustained 2nd phase. The mechanisms underlying biphasic insulin release remain only partially elucidated. First phase release can be evoked by any pharmacological compound or fuel molecule that has the capacity to increase cytosolic Ca^{2+}, whereas 2nd phase is only observed in response to metabolizable fuel stimuli (6,7). Similar distinct components of insulin release are also observed in voltage-clamped single β-cells; a rapid exocytotic burst lasting ~ 500–1000 ms that is followed by insulin exocytosis at much lower rates (8–10). The exocytotic burst reflects the release of insulin granules that are fully primed for exocytosis (readily releasable pool; RRP) and require only Ca^{2+} to be discharged, whereas the second component of exocytosis is energy-dependent and can only be observed in the presence of Mg-ATP. The idea that the exocytotic burst observed in single-cell experiments corresponds to the set of insulin granules released during 1st phase insulin secretion is also supported by quantitative evidence, immunoprecipitiation and imaging studies (9,11,12).

Second phase glucose-evoked insulin secretion is associated with the arrival of new insulin granules at the plasma membrane as demonstrated by studies utilizing TIRF microscopy (11). Insulin granule transport to the periphery occurs along microtubules (13,14) by ATP-dependent motor activity of the conventional kinesin KIF5B (15,16). In contrast to 1st phase insulin secretion, 2nd phase is highly temperature-sensitive (17,18). This temperature dependence of insulin secretion is also evident in single β-cells and has been demonstrated to be closely associated with priming, i.e. the final ATP-requiring reaction in exocytosis (8,19). Accordingly, cooling reduces rates of insulin granule mobilization in the single cell after the ATP-independent exocytotic burst has been completed. A potential target for the cooling-mediated suppression of insulin release is temperature-dependent inhibition of KIF5B ATPase activity.

Here we have combined live confocal imaging of clonal INS-1 cells labelled by transient expression of EGFP-chimeric granule proteins with capacitance measurements of single-cell exocytosis. Insulin granule movement was

analysed in detail to distinguish directed and random modes of insulin granule movement. By comparing the effects of temperature, glucose and microtubule depolymerization on the different modes of insulin granule movement and exocytotic capacity, we have aimed at obtaining an in-depth understanding of the basic characteristics of granule recruitment during glucose-evoked insulin secretion.

Results

Temperature-dependence of insulin exocytosis

We first explored the effects of cooling on INS-1 cell exocytotic responses (measured as increases in cell capacitance, ΔC) elicited by trains of voltage-clamp depolarizations from the holding membrane potential -70 mV to 0 mV (Figure 1A). At 34 °C the train evoked a $\sim$410 fF increase in cell capacitance. When the temperature was lowered to 24 °C, the exocytotic response was suppressed overall by >60%, an effect that was reversed (92% of initial) when returning to 34 °C (not shown). In a series of five experiments, the total increases in cell capacitance averaged 470 ± 44 fF at 34 °C and 233 ± 27 fF at 24 °C ($p < 0.01$; $n = 5$). Interestingly, when studying the exocytotic responses to the individual pulses (Figure 1B) it became apparent that the effect of cooling varied during the train. Accordingly, whereas the response to the first two depolarizations was only moderately affected, exocytosis during the remainder of the train was much more sensitive to cooling ($\sim -70\%$). This finding is consistent with our previous observations in primary β-cells that release of RRP occurs independently of temperature, whereas recruitment of new granules for release is markedly temperature-sensitive (8).

Reducing the temperature from 34 °C to 24 °C was also associated with a $\sim$15% reduction in voltage-gated Ca^{2+} influx, which was similar throughout the train. To verify a direct effect of cooling on the insulin release machinery, we next elicited exocytosis by intracellular dialysis of a Ca^{2+}/EGTA buffer-containing patch electrode solution ($[Ca^{2+}]_{i\ free} \sim 1.5\ \mu M$) using the standard whole-cell configuration (Figure 1C). Apart from the initial seconds of recording, exocytosis occurred at much slower rates at 24 °C than at 34 °C. Mean exocytotic rates during the first minute of recording amounted 24 ± 4 fF/s and 7 ± 3 fF/s at the high and low temperature, respectively ($p < 0.001$; $n = 7$ and 8, at 34 °C and 24 °C, respectively).

Temperature dependence of bulk insulin granule transport

The observation that cooling primarily affects a slow component of exocytosis that represents recruitment of new granules for release from a reserve, suggests that intragranular translocation of insulin granules may be sensitive to cooling. We assessed bulk insulin granule mobility as fluorescence recovery after photobleaching (FRAP) in confocal imaging experiments with the insulin granules labelled by targeted expression of a fluorescent EGFP-phogrin chimeric protein (20). EGFP-Phogrin inserts in the granule membrane and is recycled after exocytosis (Figure 2). After acquiring control images for comparison, regions covering $\sim 25\ \mu m^2$ at the tip of triangular ends of the cells were photobleached, which reduced EGFP fluorescence intensity by $\sim$65%. Confocal images were then acquired every 10 s to monitor insulin granules migrating into the bleached regions from other parts of the cell, reflected as the recovery of average fluorescence intensity. At 24 °C (Figure 2A,B) fluorescence recovery was markedly impaired in comparison with that observed when the temperature was maintained at 34 °C (Figure 2C,D). Average

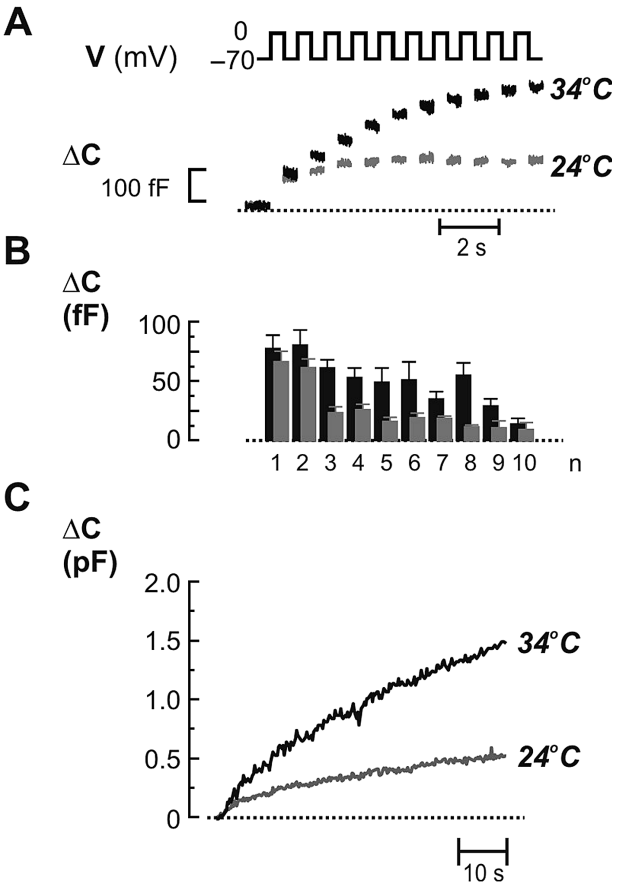

Figure 1: Temperature dependence of insulin exocytosis. A) Exocytosis monitored in a single INS-1 cell as the increase in cell capacitance (ΔC) elicted by trains of 10 500-ms voltage-clamp depolarizations from -70 mV to zero (V), at 34 °C (in black) and after lowering the temperature to 24 °C (in grey). B) Average $\Delta C \pm$ S.E.M. in response to the respective pulse in the train of depolarizations, at 34 °C (black) and after lowering the temperature to 24 °C (grey). Data represent five independent experiments (= cells). C) Exocytosis elicited by intracellular dialysis of a patch electrode solution containing a Ca^{2+}/EGTA-buffer (free $[Ca^{2+}]_i \sim 1.5\ \mu M$). The standard whole-cell configuration was established at $t = 0$. In this experiment a modified extracellular solution was used without TEA-Cl (equimolarly replaced by NaCl) and forskolin. The experiments shown are representative traces from a series of 7 and 8 recordings, made at 34 °C and 24 °C, respectively.

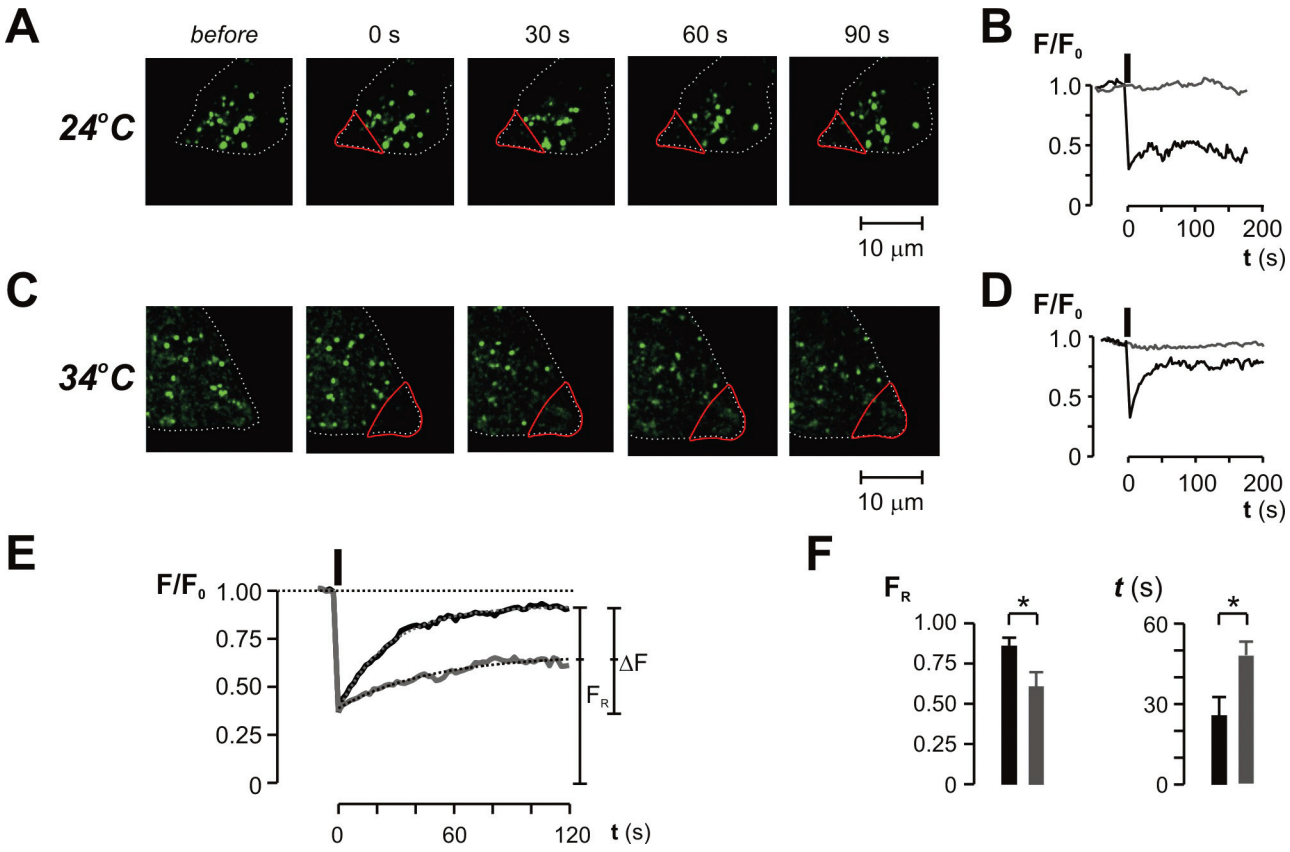

Figure 2: Temperature dependence of granular fluorescence recovery after photobleaching. A) Series of confocal images made in a single INS-1 cell at 24 °C of insulin granules fluorescently labelled by overexpressing a EGFP-phogrin chimeric protein. After acquiring a reference image (*before*), the selected region-of-interest (ROI, red) was repeatedly illuminated by high-energy excitation 488-nm laser light to photobleach the fluorescent granules within the ROI. Immediately after the bleach episode (0 s), average ROI fluorescence intensity was markedly reduced, and recovered slowly at later times (30, 60 and 90 s). B) Average fluorescence expressed as the fraction of the initial value (F/F_0) observed in the cell shown in (A) plotted vs. time, for the bleached ROI (black lower trace) and for a control nonilluminated ROI (grey upper trace). The black bar denotes the bleach episode. C and D), as in (A) and (B), but the experiment was done at 34 °C. E) Average fluorescence recovery after photobleaching at 34 °C (black trace) and 24 °C (grey trace), expressed as the fraction of the initial value (F/F_0). The black bar denotes the bleach episode. The dotted lines represent the least squares fit to the function $y = F_R - \Delta F^{(-t/t)}$ where y represents the observed F/F_0 at t seconds after cessation of photobleaching, with F_R and ΔF representing the estimated plateau levels of maximal fluorescence recovery and the amount of fluorescence recovery, respectively. The time constant for recovery is denoted as t. The data represent averages of 8 and 10 experiments, made in the cold and at 34 °C, respectively. F) Average steady-state fluorescence recovery expressed in fractions of the initial fluorescence value (F_R; left) and average estimated time constants (***t***; right). Data represents mean ± S.E.M. observed in 10 and 8 experiments made at 34 °C (black bars) and 24 °C (grey bars), respectively. *$p < 0.05$.

values of fluorescence intensities during the recovery phase were best fitted by single exponential functions at both temperatures. Steady-state fluorescence recovery was determined to 25 ± 7% and 52 ± 4% (corresponding to final fluorescence intensities of 60 ± 9% and 97 ± 5% of the initial value) at 24 °C and 34 °C, respectively ($p < 0.05$; $n = 8$ and 10, at 24 °C and 34 °C, respectively) (Figure 2E-F). The time constant for recovery averaged 47 ± 7 s and 26 ± 4 s at 24 °C and 34 °C ($p < 0.05$; $n = 8$ and 10, at 24 °C and 34 °C, respectively) (Figure 2E,F). The summed effect of these cooling-induced changes in granule mobility suggests that bulk insulin granule translocation in the cold occurs at a rate ~30% of that observed at 34 °C.

Cooling-induced effects on directed and random insulin granule movement

In order to better characterize the individual granule movements, EGFP-labelled insulin granules were then captured by time-lapse series of confocal images acquired at 5 Hz or faster followed by off-line granule tracking and movement analysis. Granule mobility at 34 °C was intense and granule velocities ranged between 100 nm/s and 1 μm/s. Two distinct modes of insulin granule movement could be directly identified by visual inspection. First, a seemingly random pattern of insulin granule movement by which net granule displacement normally was limited to < 1 μm over 1 min of imaging. Second, a much faster mode of insulin granule translocation by which the granules covered several μm in

a few seconds. Frequently, the same insulin granule exhibited both modes of granule movement (Figure 3A). To determine quantitatively whether the movements were random or directed, the mean squared displacement (MSD) was calculated for all tracks for time periods up to 10 s. Movements were defined as directed if the MSD values were best fitted by a second degree function (Figure 3B), whereas granules where MSD was best described by a linear function were taken to represent random movements (Figure 3C). Directed insulin granule mobility was quantified by counting the number of events detected per cell and minute, as well as by determining the average granule velocity. Random movement was quantified as the cell average of the granule diffusion coefficients (*D*).

Given the marked temperature sensitivity of bulk insulin granule transport (Figure 2), the effects of cooling on the distinct modes of insulin granule movement were investigated in detail in parallel with capacitance measurements of exocytosis. First, in agreement with the results in Figure 1, reducing the temperature from 34 °C to 24 °C selectively suppressed a sustained component of exocytosis, while leaving an initial component of exocytosis unaffected (Figure 3D,E; $p < 0.01$, when comparing *total* increases in cell capacitance elicited at 24 °C and 34 °C, $n = 14$). Second, the number of fast directed insulin granule movements decreased drastically by 85% from 11.1 ± 0.4–1.7 ± 0.2 per cell and minute ($p < 0.001$, $n = 14$) and events detected in the cold were 25% slower than the ones measured at 34 °C (669 ± 61 nm/s and 503 ± 66 nm/s, at 34 °C and 24 °C, respectively; $p < 0.001$, $n = 14$; Figure 3F,H). Interestingly, random diffusional activity was also suppressed and the average diffusion coefficient (*D*) decreased by 51% (from $13.1 * 10^{-14}$ m^2/s at 34 °C to 6.4 10^{-14} m^2/s; $p < 0.001$, $n = 14$; Figure 3G,I).

Relation between random insulin granule diffusion and directed granule translocation

To achieve a more complete characterization of the temperature sensitivity of the different aspects of insulin granule movement, confocal time-lapse imaging was performed at 24 °C, 29 °C and 34 °C and the image series were analysed to quantify diffusional activity as well as directed insulin granule movement (Figure 4A). Directed granule translocational activity (events/cell and minute) decreased by 58%, from 10.8 ± 0.7 to 4.6 ± 0.3 events/cell and minute when reducing the temperature from 34 °C to 29 °C, and by a further 63% to 1.6 ± 0.3 when the temperature was lowered to 24 °C, corresponding to an overall 84% decrease in the temperature range investigated ($n = 25$; $p < 0.001$ for both temperature changes). Mean velocities were less affected and decreased by 12% and 16%, in response to the respective temperature changes (average velocities 639 ± 29, 562 ± 26 and 469 ± 16 nm/s, at 34 °C, 29 °C and 24 °C, respectively; $p \sim 0.05$ and $p < 0.01$ for the respective temperature changes). Random granule diffusion was also markedly temperature-sensitive and average diffusion coefficients decreased by 35% and 36% when the temperature was reduced from 34 °C to 29 °C, and then further down to 24 °C, respectively (average *D* 14.8×10^{-14}, 9.6×10^{-14} and 6.1×10^{-14} m^2/s, at 34 °C, 29 °C and 24 °C, respectively; $p < 0.001$, for both temperature changes).

The temperature-dependent effects on insulin granule movements were further analysed by constructing Arrhenius' plots (Figure 4B), from which the energy of activation (E_A) can be derived. We thus estimated that the overall 27% reduction in average granule velocities obtained by reducing the temperature from 34 °C to 24 °C corresponds to an E_A of only ~ 22 kJ/mol. The stronger suppressive action of cooling on the frequency of directed events and the diffusion coefficients was reflected as higher estimates of E_A that were ~ 135 kJ/mol and ~ 60 kJ/mol, respectively. We then plotted the number of events detected in an individual cell vs. the average diffusion coefficient measured in that particular cell (Figure 4C). This analysis revealed a clear correlation between directed translocational activity and diffusional activity at the single-cell level. When the number of events per individual cell was instead plotted against the average directed granule translocation velocities (Figure 4D), a similar correlation could not be observed.

Insulin granule movement during glucose-stimulated insulin secretion

To compare the temperature-dependent effects on granule movement with those observed under physiological conditions, we next assessed the effects of elevating the glucose concentration. Addition of glucose (10 mM) to the extracellular medium elevated cytosolic $[Ca^{2+}]_i$ within ~ 1 min from the basal average 245 ± 37 nM to 703 ± 31 nM, where it remained ($p < 0.05$; $n = 5$; Figure 5A). Insulin granule mobility was already noticeable in the absence of glucose (30 min after removal of the sugar) and 11.8 ± 1.2 events ($n = 22$) were detected per cell and minute, exhibiting an average velocity of 496 ± 44 nm/s (Figure 5B,C). Insulin granule mobility was not abruptly affected by increasing extracellular glucose, but instead accelerated slowly. Steady-state was achieved 15 min after addition of the sugar, when the number of directed insulin granule translocations had increased by 22% to 14.6 ± 0.6 per cell and minute ($p < 0.05$ vs. in the absence of glucose), paralleled by a 47% acceleration in average granule velocities (718 ± 79 nm/s; $p < 0.05$). Random granule movement was only marginally affected by glucose and the mean diffusion coefficient (*D*) increased by 12% (n.s) from $14.5 \pm 1.6 * 10^{-14}$ m^2/s to $17.4 \pm 1.9 * 10^{-14}$ m^2/s in response to glucose (Figure 5D,E).

Effects of microtubule disruption on insulin granule movement and exocytosis

We then investigated the role of the microtubule system for directed insulin granule movement and insulin

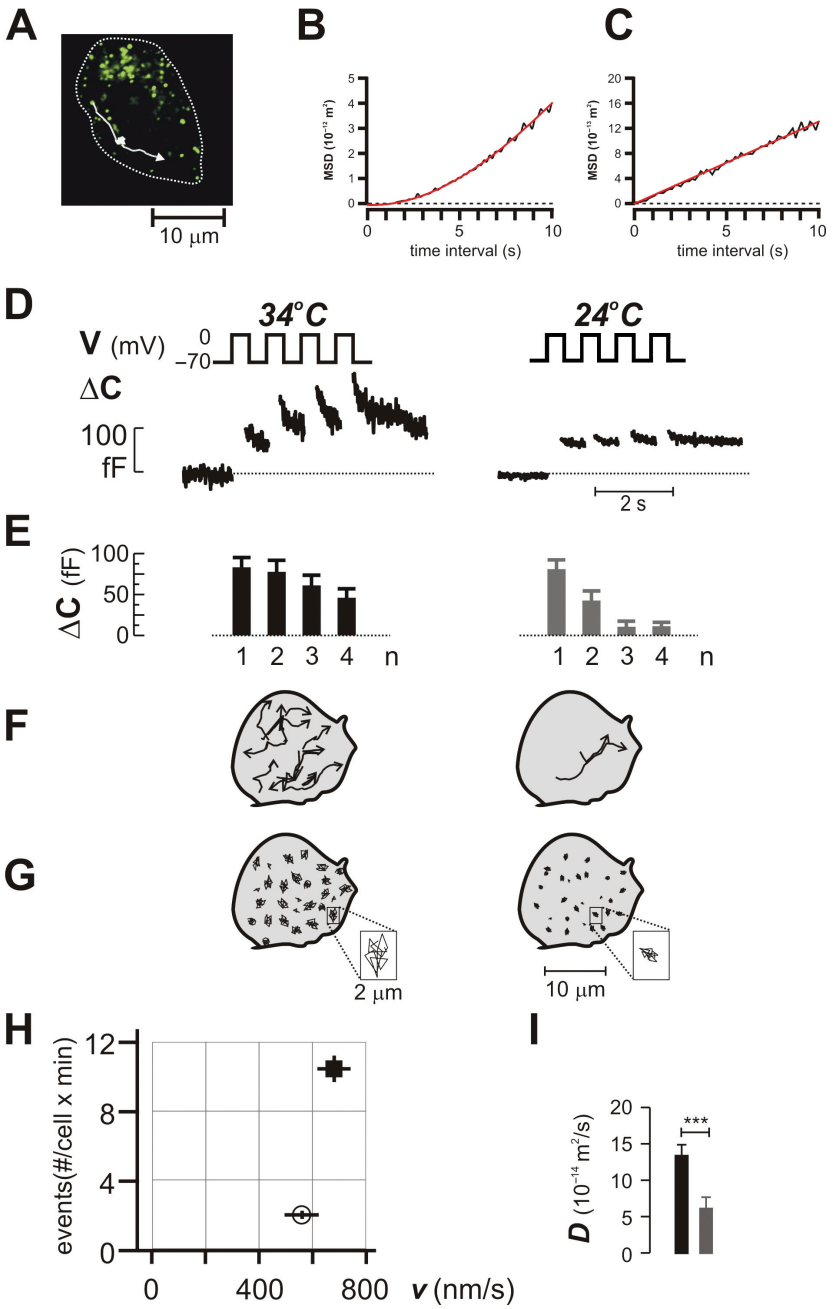

Figure 3: Analysis of granule movement and effects of cooling on directed and random granule mobility. A) Confocal image of a cell with insulin granules labelled by overexpression of an emerald-IAPP fusion protein that localises to the granule interior and is coreleased with insulin. The white trace presents one example of granule motion behaviour. The granule was tracked for 40 s, during which it underwent initial directed movement, interrupted by 15 s of seemingly random jostling, before embarking on a final directed event. B) Example of a directed granule movement as evidenced by analysis of mean squared displacement (MSD) over time intervals up to 10 s. The red curve represents the second degree equation that was best fitted to the observed MSD values. C) As in (B), but the MSD values were instead best described by a linear function, indicating that the granule moved by random diffusion. Note the different scaling for the MSD values in (B) and (C). D) Increases in cell capacitance (ΔC) evoked by trains of depolarizations (V) at 34 °C and immediately after lowering the temperature to 24 °C, as indicated. These traces are representative of a series of 14 experiments. E) Average ΔC ± S.E.M. in response to the respective pulse in the train of depolarizations observed in 14 cells before (black) and immediately after reducing the temperature from 34 °C to 24 °C (grey). F) Directed insulin granule movements recorded in the same cell as in (D) at 34 °C and immediately after lowering the temperature to 24 °C, as indicated. G) Random granule movements under the same conditions as in (F). Examples represent a random (and representative) selection. H) Frequency of directed granule movements (events) plotted vs. the directed granule movement velocity (v). The data represent the averages ± S.E.M. of 14 experiments done at 34 °C (■) and immediately after reducing the temperature to 24 °C (○). I) Average diffusion coefficients (*D*) ± S.E.M. observed in the warm (black bar) and at 24 °C (grey bar). *** $p < 0.001$.

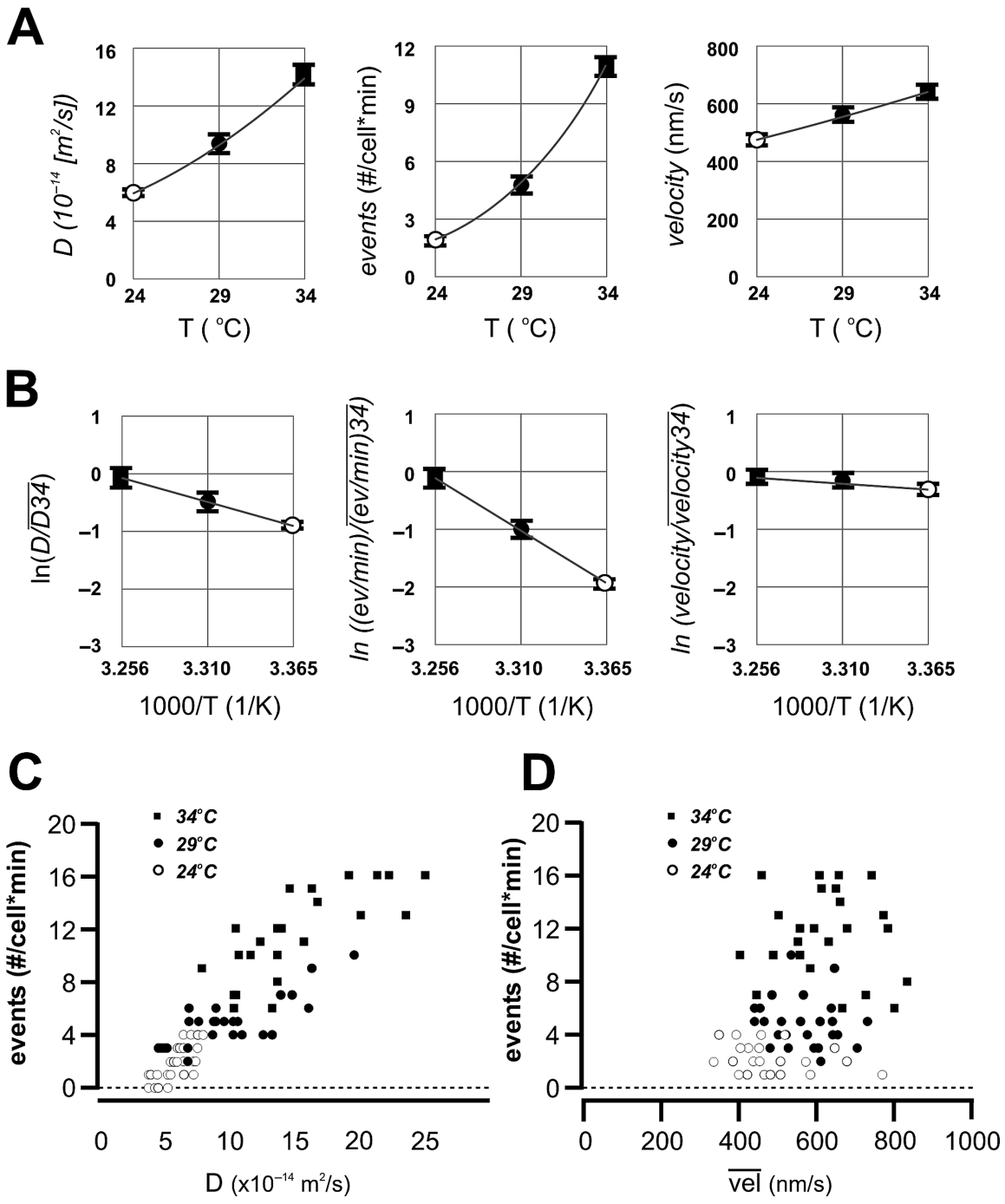

Figure 4: Activation energies and relationship between random and directed insulin granule movement. A) Diffusion coefficients (*D*), frequency of directed granule movements (*events*) and directed granule velocities (*velocity*) observed at 24 °C (○), 29 °C (●) and 34 °C (■), as indicated. B) Arrhenius plots of the effects of temperature on diffusion coefficient (*D*), directed translocational activity (*ev*) and directed granule velocities (*velocity*). To allow for comparison of the temperature dependence of the different entities, rates have been normalised to the means observed at 34 °C. The grey lines represent the least-squares fit of the data to the equation: $ln\,k = lnA - E_A/RT$, where k represents the relative change in reaction rate at the respective absolute temperature, A is the pre-exponential factor and R and T have their usual meanings. Values for E_A thus estimated for *D*, events and velocities were ~60 kJ/mol, ~135 kJ/mol and ~22 kJ/mol, respectively. C) Frequency of directed granule movements (events) observed in a single cell plotted vs. the diffusion coefficient (*D*) measured in the same cell, for all cells at all temperatures in the series. ○, ● and ■ refer to data obtained at 24 °C, 29 °C and 34 °C, respectively. D) As in (C) but directed translocational activity (events) was instead plotted vs. the average directed granule velocitiy (vel). Note the correlation between events and *D* in (C), and the poor predictive value of the directed granule velocity (vel) for directed translocational activity (events) apparent in (D).

exocytosis. Microtubules were observed throughout the entire INS-1 cell volume (Figure 6A), consistent with findings in other clonal β-cells (MIN6 (16)). Pre-treatment with the microtubule inhibitor vindesine (1 μM, > 60 min) collapsed the microtubule cytoskeleton (Figure 6B), which reduced the rapid and sustained components of depolarization-evoked exocytosis by ~50% in a symmetrical fashion (Figure 6C; $p < 0.001$; $n = 21$ and 12, with or without vindesine treatment, respectively). Interestingly, exocytosis was not rapidly exhausted in vindesine-treated cells, but remained at ~50% of that observed in untreated cells when the train stimulation was repeated every second minute for up to 10 min.

Insulin granule mobility was severely affected by microtubule disruption. The frequency of fast directed granule translocations dropped dramatically by 85% ($p < 0.001$; $n = 21$ and 12, with or without vindesine treatment, respectively). For the few directed granule translocations that could still be observed, the velocities were similar to those measured in untreated cells (Figure 6D, F). By contrast, diffusive granule movement was not much affected (Figure 6E, G). To directly assess the role of microtubules for directed insulin granule movement we then visualised the microtubule system using an EGFP-tubulin chimera in combination with the acidotropic dye LysotrackerRed, which probes the insulin granules and other acidic organelles. Fast directed granule movements could invariably only be detected along the microtubules (See appendix 1 at http://www.traffic.dk/videos/5_10.asp), in agreement with previous reports in MIN6 cells (16).

Limits for diffusion of the single granule

The previous set of experiments in Figure 6 showed that insulin exocytosis is maintained in the absence of functional microtubules. Therefore we finally wanted to investigate how far an insulin granule can move by mere diffusion. To this end we selected confocal image series

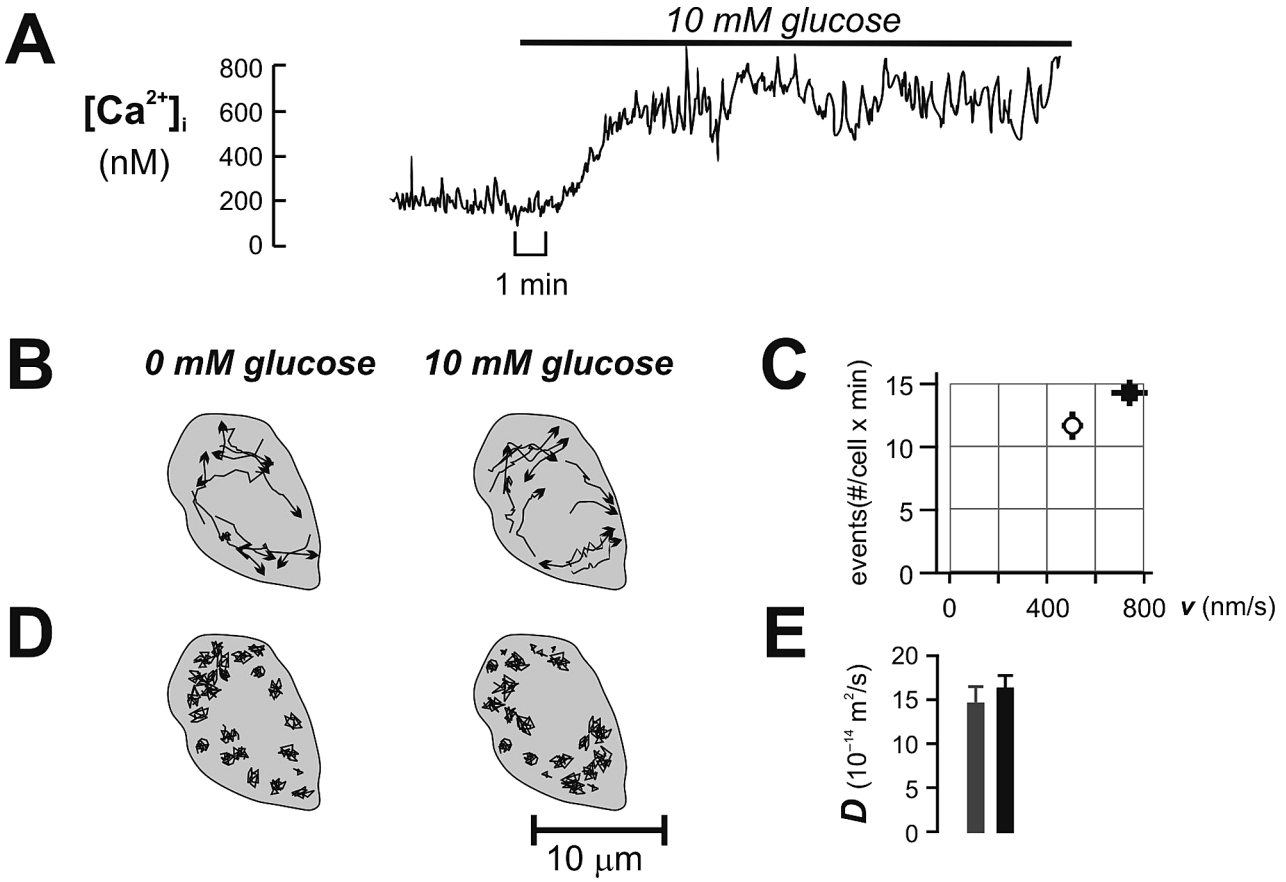

Figure 5: Effects of glucose on insulin granule movement. A) Cytosolic Ca^{2+} concentrations before and after addition of 10 mM glucose in an INS-1 cell. This recording is representative of a series of five independent experiments. B) Trajectories representing the directed events detected during 1 min of imaging in the absence or presence of glucose, as indicated. C) Frequency of directed granule movements (events/cell*min) plotted vs. the directed granule movement velocity (*v*). The data represent the averages ± S.E.M. in 22 experiments observed in the absence of glucose after a 30-min preincubation period (○) and 15 min after elevating the glucose concentration (10 mM; ■)., respectively. D) Trajectories for granules moving by random diffusion observed under the same conditions as in (B). For the sake of clarity, not all diffusive movements are shown, and the examples represent a random (and representative) selection. E) Average diffusion coefficients (*D*) ± S.E.M. observed in the absence (grey bar) and presence of glucose (black bar), respectively, in 22 experiments.

in which insulin granules could be tracked for at least 1 min and calculated the MSD for the entire period. It then became apparent that granule diffusion is overall restricted and MSD values rapidly plateaued for longer time intervals (Figure 7A,B). At 34 °C this plateau occurred when the time period was extended to 30 ± 5 s. The average MSD was estimated by calculating the net displacement corresponding to the plateau, multiplying this by two and adding one average granule diameter (Figure 7C). It was thus determined to be 0.88 ± 0.09 μm ($n = 14$ (cells)) at 34 °C. Disruption of the microtubule system increased the average maximal distance by which the granule can move by

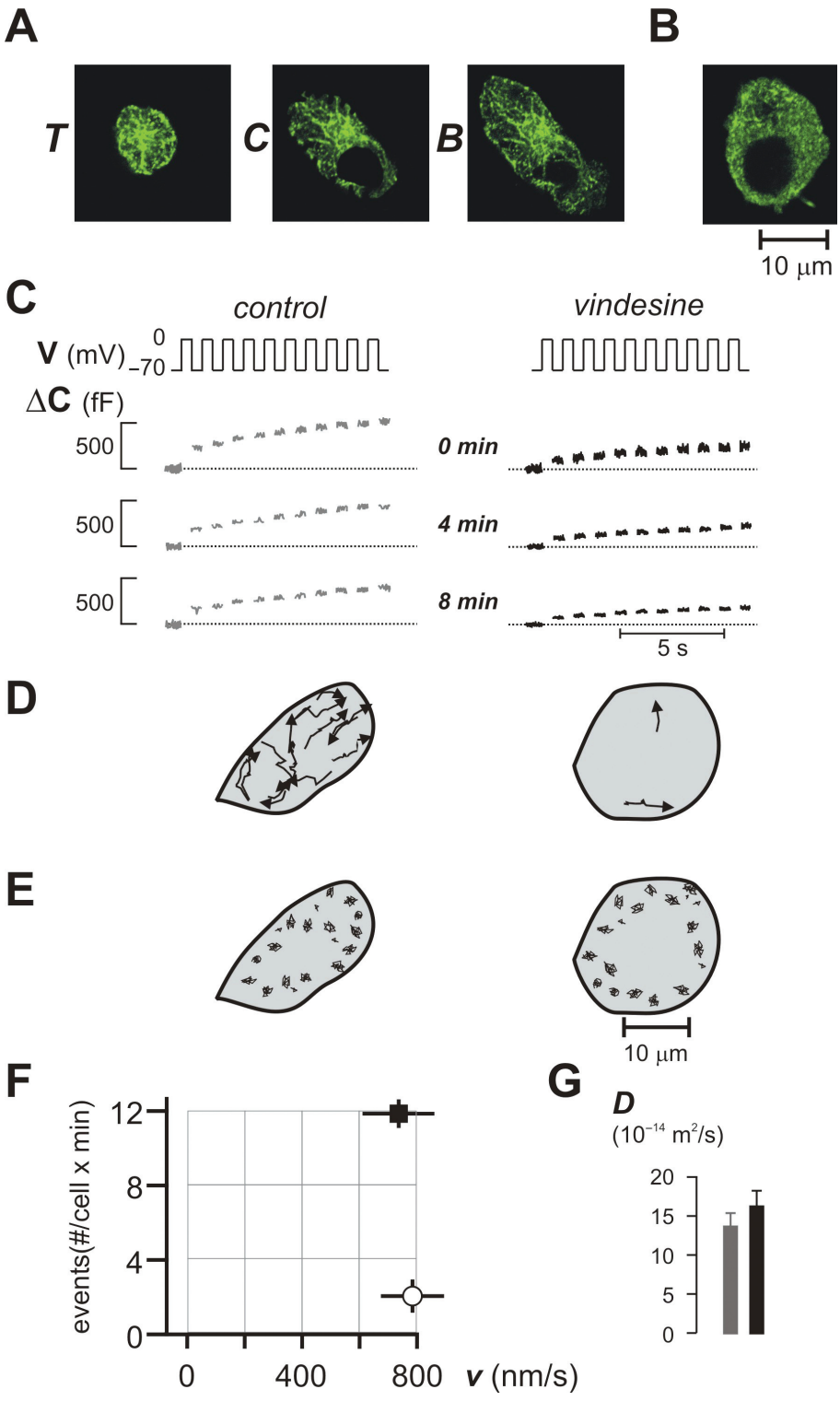

Figure 6: Effects of micro-tubule disruption on insulin exocytosis and granule movement. A) Confocal images of α-tubulin immunoreactivity from top (*T*), central (*C*) and bottom (*B*) sections of an INS-1 cell. B) Same as in (A) but from a central section of the cell after pretreatment with the mictotubule inhibitor vindesine (1 μM, > 60 min). C) Increases in cell capacitance (ΔC) evoked by trains of depolarizations (V) in an untreated control cell (grey) and in a vindesine-treated cell (black). Train stimulations were applied every second minute after the first stimulation, shown here are responses recorded after 4 and 8 min. These traces are representative of a series of 12 and 21 experiments, in control and vindesine-treated cells, respectively. D) Directed insulin granule movements in a control and a vindesine-treated cell. E) Random granule movements under the same conditions as in (D). Examples represent a random (and representative) selection. F) Frequency of directed granule movements (events/cell*min) plotted vs. the directed granule movement velocity (*v*). The data represent the averages ± S.E.M. in 12 and 21 experiments made in untreated control cells (○) and in vindesine-treated cells (■). G) Average diffusion coefficients (*D*) ± S.E.M. observed in 12 untreated control cells (grey bar) and in 22 vindesine-treated cells (black bar).

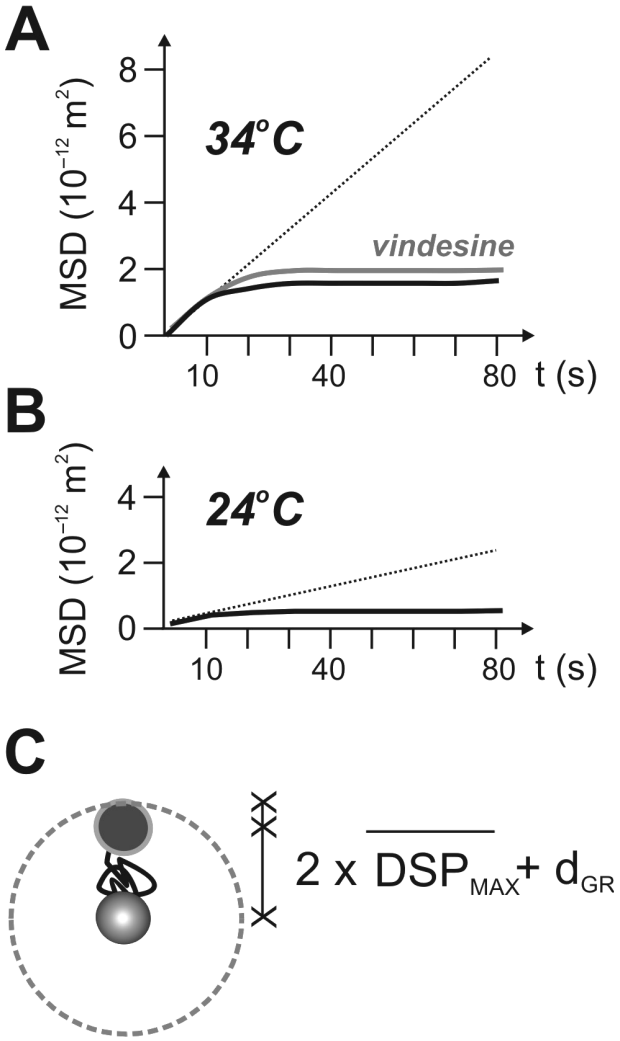

Figure 7: Restrictions to insulin granule diffusion. A) The least-squares fit to the mean squared displacement (MSD) of two insulin granules observed at 34 °C in untreated control cells (black trace) and in cells pretreated with the microtubule inhibitor vindesine (1 μM, > 60 min; grey trace). At variance with previous MSD analyses (Figures 3–6), only granules that revealed a random type of movement and that could be tracked for periods > 60 s were studied. This analysis revealed that insulin granule diffusion is overall restricted, reflected by the MSD values reaching a plateau after ~30 s. The hatched line denotes the predicted MSD development, had diffusion continued in an unrestricted mode. B) As in (A), but the data was obtained at 24 °C. C) The average maximal displacement (DSP_{MAX}) by diffusion, derived from the values of the MSD plateaux for the individual granules, and the average granule diameter (d_{GR}) were used to estimate the size of functional 'cages' for insulin granule diffusion. Average values of 'cage' sizes thus obtained under the respective conditions are presented in the text.

diffusion by 27% to 1.15 ± 0.35 μm ($p < 0.01$ vs. untreated cells, $n = 14$ and 12, in untreated and vindesine-treated cells, respectively; Figure 7A). At 24 °C, diffusional movement was slower, but also more restricted. Under these conditions, an insulin granule could on average only drift 0.58 ± 0.06 μm by diffusion before further displacement was blocked ($p < 0.001$ vs. at 34 °C, $n = 14$ in both groups; Figure 7B).

Discussion

Rapid 1st phase insulin secretion primarily reflects the discharge of insulin granules predocked to the plasma membrane (RRP; readily releasable pool), whereas the slower but sustained 2nd phase is associated with the arrival of new insulin granules at the plasma membrane and acceleration of microtubule-dependent insulin granule transport (11,15,20). In this study we have made use of the high temperature sensitivity of 2nd phase insulin secretion to address some fundamental properties of insulin granule transport during glucose-stimulated insulin release. In the following we will discuss why kinesin- and microtubule-dependent insulin granule transport is unlikely to represent the bottleneck that creates the nadir of phasic insulin release. Instead, we will highlight the importance of random insulin granule diffusion at both proximal and distal stages of insulin secretion.

Directed and random insulin granule movement

Insulin granule mobility has by now been the focus of several studies (11,15,16,20–23). These studies have invariably assessed either bulk insulin granule translocation or dealt with various aspects of the role of directed granule movement in insulin secretion. A seemingly random type of granule jostling has also been reported (20) but has not yet been analysed in depth. Granule diffusion as quantified by determining the mean diffusion coefficient D over time intervals up to 10 s, typically produced values $\sim 12 \times 10^{-14}$ m^2/s, corresponding to a net ~2.6 μm displacement over a minute, if diffusion is without constraints. However, when extending the time intervals for the MSD analysis, it is clear that diffusion is overall restricted and the average maximal displacement by mere diffusion is actually attained after ~30 s and occurs within functional 'cages' of ~0.9 μm diameter (cf. Figure 7).

The importance of microtubule-guided granule transport in insulin secretion was established by electron microscopy (14), secretion studies (24) as well as phase contrast imaging in foetal rat islet cell monolayers (23). The colabelling experiments shown here using EGFP-tubulin and LysoTrackerRed confirm that in INS-1 cells, as in MIN6 cells (16), directed insulin granule movement occurs exclusively along the cytoskeleton (See appendix 1 at http://www.traffic.dk/videos/5_10.asp). The directed granule translocation velocities observed in the present study (100 nm/s up to 1 μm/s) are similar to those previously reported by others (15,20,23). Additionally, we occasionally observe a small population of considerably faster granule translocation events with velocities of 1–3 μm/s that was previously only reported by Varadi et al. (16). Interestingly, disruption of the microtubule system by vindesine dramatically

suppressed directed insulin granule movement by >80%, whereas the inhibition of exocytosis was limited to ~50% (Figure 6C). With the observation that insulin exocytosis is not rapidly exhausted in vindesine-treated cells, this could be interpreted as indicating that a considerable proportion of insulin granules is able to reach the plasma membrane by mere diffusion. It should be pointed out that diffusion may also occur with the granules attached to the microtubules, reflecting microtubule remodelling.

Random insulin granule movement controls directed granule transport

Cooling severely affects insulin granule transport and the >80% reduction in the frequency of directed insulin granule translocations (Figures 3 and 4) is in close agreement with the estimated ~70% reduction in bulk granule translocation rates as suggested by the FRAP experiments (Figure 2). Perhaps the most intriguing observation made in this study is the much stronger effect of reducing the temperature from 34 °C to 24 °C on the frequency of directed events (>80% reduction) than on average velocity of directed granule movement (25% reduction; Figures 3H and 4). This is at variance with the effects of removing glucose from the extracellular medium, which reduces mean directed granule velocity by ~30%, similar to the effect of cooling, whilst having a much more moderate ~20% effect on the frequency of directed events (Figure 5B,C). Furthermore, when estimating the temperature sensitivity of directed granule velocities (reflecting kinesin ATPase activity and processivity) by deriving the energy of activation (E_A; Figure 4B) this produced a value ~22 kJ/mol (slightly less than that determined for single kinesin molecules in bead assays (25)), which is much lower than the estimated E_A 135 kJ/mol for the frequency of directed events. The latter value is, however, in good agreement with the 145 kJ/mol previously determined for 2nd phase insulin release (8,17).

These comparisons strongly support the idea that the dramatic cooling-induced suppression of directed granule translocation and insulin release is not caused by a temperature-dependent reduction in kinesin ATPase activity, but is rather the result of another process, such as temperature-dependent granule diffusion. It is not hard to envision that attenuated granule diffusion may perturb granule redirection and switching between different microtubules before embarking on a kinesin-driven translocation. This possibility seems likely given that diffusional activity in the individual cell clearly correlates with the number of directed granule translocations (Figure 4C), whereas kinesin activity (as reflected by average directed granule velocities) only poorly predicts the frequency of directed events in the single cell (Figure 4D).

Roles of random and directed modes of granule movement in phasic insulin secretion

We report here that, in agreement with previous data (15,20), elevation of the extracellular glucose concentration stimulates microtubule-guided directed insulin granule movement at time points corresponding to the onset of 2nd phase insulin secretion (Figure 5). The fact that 2nd phase insulin secretion is dependent on β-cell metabolism makes ATP-dependent kinesin-driven granule translocation along the microtubules an obvious candidate for the reaction that restricts the rate of insulin secretion after completion of the 1st phase. Indeed, it has previously been reported that a dominant-negative KIF5B mutant selectively suppresses the 2nd phase in clonal insulin-releasing MIN6 cells (15). However, it should be emphasized that microtubule-dependent directed insulin granule trafficking is a constantly ongoing process and even in the absence of glucose proceeds at ~60% of that observed during 2nd phase (estimated by combining the 22% increase in frequency of directed events and the 47% acceleration of mean granule velocity). In addition, although disruption of the microtubule system results in a dramatic 85% suppression of directed insulin granule movement, a fast as well as a slow component of exocytosis can repeatedly be elicited by trains of depolarizations (Figure 6C). This clearly suggests that the basic mechanisms creating the biphasic insulin release pattern are still operational in the absence of a microtubule system. Similarly, the use of microtubule inhibitors in studies investigating the phasic nature of insulin release has produced ambiguous results (13,24,26,27).

By contrast, cooling affects the insulin release kinetics and selectively suppresses the ATP-dependent 2nd phase whilst leaving the ATP-independent 1st phase secretion unaffected (Figures 1 and 3D-E) (17,18). This, taken together with the fact that the cooling-induced reduction in insulin granule mobility is caused by inhibition of diffusional granule movement, points to the conclusion that insulin granules released during 2nd phase (as opposed to granules released during 1st phase) must translocate by diffusion prior to exocytosis.

In conclusion, our results are suggestive of a paradoxical scenario in which a basically unregulated mechanism such as granule diffusion determines the extent of a tightly controlled process such as phasic insulin secretion. However, the β-cell is in fact equipped with excellent means to control the extent of granule diffusion during the distal passage of the dense peripheral actin web (14,28). Similarly, exact biological control of all the different stages of the insulin release machinery can be achieved by fine-tuning the basic conditions for granule diffusion in subcellular regions of the β-cell.

Materials and Methods

Cell culture and transfection procedures

All experiments were performed in clonal insulin-releasing INS-1 cells. Cells were cultured in RPMI 1640 medium

(11 mM glucose; Gibco BRL, Invitrogen, Sweden) supplemented with 10% foetal calf serum (FCS), streptomycin (100 μg/mL), penicillin (100 μg/mL) and 2-mercaptoethanol (50 μM). For labelling of insulin granules, cells were plated on glass coverslips and transfected with different markers using Effectene Transfection Reagent (Qiagen, VWR, Sweden). Two different fluorescent fusion proteins were used as granule markers: EGFP-phogrin, which localizes to the insulin granule membrane (20), and emerald-IAPP (islet amyloid polypeptide). Emerald is a pH-insensitive version of EGFP and the chimeric protein localizes to the granule interior and is released upon exocytosis (29). For colabelling of microtubules and granules (See appendix 1 at http://www.traffic.dk/videos/5_10.asp) cells were first transfected with EGFP-tubulin (Clontech, BD Biosciences, Stockholm, Sweden) and then stained with LysotrackerRed (Molecular Probes, Leiden, the Netherlands), an acidotropic fluorescent marker that localizes within acidic compartments, such as the secretory granules.

Immunocytochemistry

INS-1 cells cultured on coverslips were fixed in 4% formaldehyde in PBS and permeabilized with 0.1% Triton X100. After blocking of nonspecific binding with 5% normal donkey serum, cells were first incubated for 2 h with an anti-α-tubulin antibody (Chemicon International, Temecula, CA) at a 1 : 50 dilution and then incubated for 1 h with a Cy2-conjugated secondary antibody (Pierce, Rockford, IL) at a 1 : 150 dilution. Immunoreactivity was visualised by confocal immunocytochemistry using the same settings as described in the *Confocal Imaging* methods section.

Electrophysiology

INS-1 cells were plated in 35-mm Nunc plastic Petri dishes that were later used as the experimental chamber. The measurements were conducted using an EPC-9 (Figures 3 and 6) or EPC-10 (Figure 1) patch-clamp amplifier in conjunction with the Pulse software suite (version 8.53; HEKA Elektronik, Lambrecht/Pfalz, Germany). Exocytosis was monitored as increases in cell capacitance (8,30) using the sine + DC mode of the lock-in amplifier included in the Pulse software suite. The volume of the experimental chamber was reduced to ~1.5 mL by a plastic insert and the chamber was continuously perfused (6 mL/min) and the temperature maintained at 34 °C unless otherwise indicated. The standard extracellular bath solution contained (in mM) 118 NaCl, 20 TEA-Cl, 5.6 KCl, 2.6 $CaCl_2$, 1.2 $MgCl_2$, 3 glucose, 5 HEPES and 2 μM forskolin (pH 7.4 with NaOH). The K^+ channel blocker TEA-Cl was used to block voltage-gated K^+ currents that would otherwise obscure the considerably smaller voltage-gated Ca^{2+}-currents. Forskolin was added from a DMSO stock solution (final concentration 0.01%) to promote exocytotic responses. In the parallel recordings of exocytosis and granule movement (Figure 3), TEA-Cl was equimolarly replaced by NaCl and forskolin was omitted from the extracellular solution. The experiments in which exocytosis was evoked by trains of voltage-clamp depolarizations (Figures 1A, 3 and 6) were made using the perforated-patch whole-cell approach (~intact cells), using a pipette solution consisting of (in mM) 76 Cs_2SO_4, 10 NaCl, 10 CsCl, 1 $MgCl_2$, 5 HEPES (pH 7.35 with CsOH) and 0.24 mg/mL amphotericin B. When eliciting exocytosis in the standard whole-cell configuration, in which the pipette solution dialyses the cell and replaces the cytosol (Figure 1C), the pipette solution consisted of (in mM) 125 K-glutamate, 10 KCl, 10 NaCl, 1 $MgCl_2$, 5 HEPES, 3 Mg-ATP, 10 EGTA and 9 $CaCl_2$, 0.1 cAMP and 0.05 EGTA (pH 7.2 with KOH). The resulting free intracellular Ca^{2+} concentration was estimated to 1.5 μM using the binding constants of Martell & Smith (31).

Confocal imaging

Insulin granules labelled with EGFP or the pH-insensitive EGFP variant Emerald were visualised by time-lapse confocal imaging using a Zeiss 510 LSM confocal microscope and a Plan-Apochromat 100×/1.4 oil objective. Insulin granule fluorescence was excited using the 488-nm line of the Argon-laser and emitted light was collected using a 505–530 nm bandpass filter. Images were acquired at ~5 Hz or faster. All experiments were performed with the same perfusion system as used for the electrophysiological experiments, and an extracellular bath solution consisting of (in mM) 138 NaCl, 5.6 KCl, 2.6 $CaCl_2$, 1 $MgCl_2$, 5 HEPES and 3 glucose preheated to 34 °C unless otherwise specified. The FRAP experiments (Figure 2) were done using the photobleach option of the LSM 510 software package. Photobleaching of the selected region-of-interest (ROI) was achieved by 10–20 scans with maximal intensity of the 488-nm laser excitation light. This repeatedly produced a ~65% reduction in average fluorescence intensity within the ROIs. The remaining fluorescence is likely to represent resistant background autofluorescence, and was unaffected by increasing the number of scans during the bleach period.

Granule movement analysis

Analysis of granule movements was performed off-line. The insulin granule movements were tracked using freeware from DRBIO, Cornell University, NY. The resulting trajectories were analyzed and typed in MATLAB (version 6.1.0.450; MathsWorks Inc., Boston, MA). The MSD for the initial 10 s of the trajectories was calculated according to the formula:

$$MSD(n\Delta t) = \frac{1}{N-n}\sum_{i=1}^{N-n}[\vec{r}(t_{i+n}) - \vec{r}(t_i)]^2, \qquad (1)$$

where Δt denotes the sampling time; n denotes the number of sequential sampling points (or time intervals) included ($n = 0, 1, 2 \ldots N$); $\vec{r}(t_i)$ is the location of a granule at time $t_i = i\Delta t$. To determine the type of motion of the individual granules, MSD was plotted vs. the number of time-intervals $n\Delta t$ included. Three principally different types of motion patterns could thus be identified:

- free planar diffusion, when the MSD plot was best fitted by a linear equation;
- directed planar movement, when the MSD plot was best fitted by a second degree equation;
- restricted movement, when the MSD data quickly reached a plateau (within a number of time intervals corresponding to <10 s).

For the granules moving in a random fashion, the diffusional activity during the time period was quantified as the mean diffusion coefficient (D) according to:

$$D = \frac{r^2}{4t}, \quad (2)$$

where r^2 represents the mean squared displacement during the time interval $t = n\Delta t$. In Figure 7, MSD analysis was confined to the granules that could be tracked for > 60 s and values for the estimated functional 'cage' sizes were derived by calculating the net displacements corresponding to the restriction plateaux, multiplied by 2 and with the average INS-1 cell granule diameter added(150 nm; Dr Lena Eliasson, Lund University, Sweden, personal communication).

Granules exhibiting directed granule movements could not be automatically tracked for extended periods and were therefore analyzed manually using the MetaMorph software (version 6; Universal Imaging Corporation, Downingtown, PA). The number of directed granule movements occurring per cell and minute were counted and were expressed as mean values ± S.E.M. in n cells. Granule velocities were measured during the 1-s period of the trajectories displaying the fastest movements. The rationale for doing this comes from the enormous variation in granule velocities during the tracks, which often included periods when the granules slowed down for several seconds before accelerating again (cf. Figure 3A). Path lengths, final displacement and directional changes in the tracks were also analyzed, but were not different under the respective conditions, unless when mentioned.

Microfluorimetry

$[Ca^{2+}]_i$ in INS-1 cells was measured by dual-wavelength microfluorimetry using the membrane-permeable ratiometric Ca^{2+}-indicator fura-2-AM (30 min preloading in 5 μM) and a D104 PTI microfluorimetry system (Monmouth Junction, NJ). All experiments were made at 34 °C. Calibration of the fluorescence signal was performed as detailed in (32).

Statistical analysis

All data are given as average values ± S.E.M. Statistical significance was evaluated by independent (Figures 1C, 2, and 6) or paired (Figures 1A,B, 3 and 5) Student's *t*-test, or in combination with ANOVA when comparisons involved more than two groups (Figure 4).

Acknowledgments

This work was supported by grants from the Swedish Research Council (grants no. 12234, 13509), The European Foundation for the Study of Diabetes, The Hain Foundation, The Albert Påhlsson Foundation, The Novo-Nordisk Foundation, The Swedish Diabetes Association and the Crafoord Foundation. The study would not have been possible without Prof Patrik Rorsman generously providing equipment and personnel financed by grants from the Swedish Research Council (8647AS), The Swedish Diabetes Association, FRN and the NovoNordisk Foundation. G.A.R. was supported by a Wellcome Trust Programme grant and Research Leave Fellowship.

References

1. Schulla V, Renstrom E, Feil R, Feil S, Franklin I, Gjinovci A, Jing XJ, Laux D, Lundquist I, Magnuson MA, Obermuller S, Olofsson CS, Salehi A, Wendt A, Klugbauer N, et al. Impaired insulin secretion and glucose tolerance in beta cell-selective Ca(v)1.2 Ca^{2+} channel null mice. EMBO J 2003;22:3844–3854.
2. Vajna R, Klockner U, Pereverzev A, Weiergraber M, Chen X, Miljanich G, Klugbauer N, Hescheler J, Perez-Reyes E, Schneider T. Functional coupling between 'R-type' Ca2+ channels and insulin secretion in the insulinoma cell line INS-1. Eur J Biochem 2001;268:1066–1075.
3. Ashcroft FM, Proks P, Smith PA, Ammala C, Bokvist K, Rorsman P. Stimulus-secretion coupling in pancreatic beta cells. J Cell Biochem 1994;55 Suppl:54–65.
4. Grodsky GM, Bolaffi JL. Desensitization of the insulin-secreting beta cell. J Cell Biochem 1992;48:3–11.
5. Nesher R, Cerasi E. Biphasic insulin release as the expression of combined inhibitory and potentiating effects of glucose. Endocrinology 1987;121:1017–1024.
6. Henquin JC. Triggering and amplifying pathways of regulation of insulin secretion by glucose. Diabetes 2000;49:1751–1760.
7. Gembal M, Gilon P, Henquin JC. Evidence that glucose can control insulin release independently from its action on ATP-sensitive K^+ channels in mouse B cells. J Clin Invest 1992;89:1288–1295.
8. Renstrom E, Eliasson L, Bokvist K, Rorsman P. Cooling inhibits exocytosis in single mouse pancreatic B-cells by suppression of granule mobilization. J Physiol 1996;494: (Pt 1):41–52.
9. Eliasson L, Renstrom E, Ding WG, Proks P, Rorsman P. Rapid ATP-dependent priming of secretory granules precedes Ca^{2+}-induced exocytosis in mouse pancreatic B-cells. J Physiol 1997;503: (Pt 2):399–412.
10. Barg S, Eliasson L, Renstrom E, Rorsman P. A subset of 50 secretory granules in close contact with L-type Ca^{2+} channels accounts for first-phase insulin secretion in mouse beta-cells. Diabetes 2002;51: Suppl 1: S74–82.
11. Ohara-Imaizumi M, Nakamichi Y, Tanaka T, Ishida H, Nagamatsu S. Imaging exocytosis of single insulin secretory granules with evanescent wave microscopy: distinct behavior of granule motion in biphasic insulin release. J Biol Chem 2002;277:3805–3808.
12. Daniel S, Noda M, Straub SG, Sharp GW. Identification of the docked granule pool responsible for the first phase of glucose-stimulated insulin secretion. Diabetes 1999;48:1686–1690.
13. Malaisse WJ, Van Obberghen E, Devis G, Somers G, Ravazzola M. Dynamics of insulin release and microtubular-microfilamentous system. V. A model for the phasic release of insulin. Eur J Clin Invest 1974;4:313–318.

14. Orci L, Gabbay KH, Malaisse WJ. Pancreatic beta-cell web: its possible role in insulin secretion. Science 1972;175:1128–1130.
15. Varadi A, Ainscow EK, Allan VJ, Rutter GA. Involvement of conventional kinesin in glucose-stimulated secretory granule movements and exocytosis in clonal pancreatic beta-cells. J Cell Sci 2002;115:4177–4189.
16. Varadi A, Tsuboi T, Johnson-Cadwell LI, Allan VJ, Rutter GA. Kinesin I and cytoplasmic dynein orchestrate glucose-stimulated insulin-containing vesicle movements in clonal MIN6 beta-cells. Biochem Biophys Res Commun 2003;311:272–282.
17. Atwater I, Goncalves A, Herchuelz A, Lebrun P, Malaisse WJ, Rojas E, Scott A. Cooling dissociates glucose-induced insulin release from electrical activity and cation fluxes in rodent pancreatic islets. J Physiol 1984;348:615–627.
18. Escolar JC, Hoo-Paris R, Castex C, Sutter BC. Effect of low temperatures on glucose-induced insulin secretion and ionic fluxes in rat pancreatic islets. J Endocrinol 1987;115:225–231.
19. Bittner MA, Holz RW. A temperature-sensitive step in exocytosis. J Biol Chem 1992;267:16226–16229.
20. Pouli AE, Emmanouilidou E, Zhao C, Wasmeier C, Hutton JC, Rutter GA. Secretory-granule dynamics visualized *in vivo* with a phogrin-green fluorescent protein chimaera. Biochem J 1998;333: (Pt 1):193–199.
21. Niki I, Niwa T, Yu W, Budzko D, Miki T, Senda T. Ca^{2+} influx does not trigger glucose-induced traffic of the insulin granules and alteration of their distribution. Exp Biol Medical (Maywood) 2003;228: 1218–1226.
22. Niwa T, Matsukawa Y, Senda T, Nimura Y, Hidaka H, Niki I. Acetylcholine activates intracellular movement of insulin granules in pancreatic beta-cells via inositol trisphosphate-dependent [correction of triphosphate-dependent] mobilization of intracellular Ca^{2+}. Diabetes 1998;47:1699–1706.
23. Kanazawa Y, Kawazu S, Ikeuchi M, Kosaka K. The relationship of intracytoplasmic movement of beta granules to insulin release in monolayer-cultured pancreatic beta-cells. Diabetes 1980;29: 953–959.
24. Malaisse WJ, Malaisse-Lagae F, Van Obberghen E, Somers G, Devis G, Ravazzola M, Orci L. Role of microtubules in the phasic pattern of insulin release. Ann N Y Acad Sci 1975;253:630–652.
25. Kawaguchi K, Ishiwata S. Temperature dependence of force, velocity, and processivity of single kinesin molecules. Biochem Biophys Res Commun 2000;272:895–899.
26. Farshori PQ, Goode D. Effects of the microtubule depolymerizing and stabilizing agents Nocodazole and taxol on glucose-induced insulin secretion from hamster islet tumor (HIT) cells. J Submicrosc Cytol Pathol 1994;26:137–146.
27. Malaisse-Lagae F, Amherdt M, Ravazzola M, Sener A, Hutton JC, Orci L, Malaisse WJ. Role of microtubules in the synthesis, conversion, and release of (pro)insulin. A biochemical and radioautographic study in rat islets. J Clin Invest 1979;63:1284–1296.
28. Tsuboi T, da Silva Xavier G, Leclerc I, Rutter GA. 5′-AMP-activated protein kinase controls insulin-containing secretory vesicle dynamics. J Biol Chem 2003;278:52042–52051.
29. Barg S, Olofsson CS, Schriever-Abeln J, Wendt A, Gebre-Medhin S, Renstrom E, Rorsman P. Delay between fusion pore opening and peptide release from large dense-core vesicles in neuroendocrine cells. Neuron 2002;33:287–299.
30. Ammala C, Eliasson L, Bokvist K, Larsson O, Ashcroft FM, Rorsman P. Exocytosis elicited by action potentials and voltage-clamp calcium currents in individual mouse pancreatic B-cells. J Physiol 1993;472: 665–688.
31. Martell AE, Smith RM. In: Critical stability constants. New York: Plenum Press, 1971.
32. Olofsson CS, Gopel SO, Barg S, Galvanovskis J, Ma X, Salehi A, Rorsman P, Eliasson L. Fast insulin secretion reflects exocytosis of docked granules in mouse pancreatic B-cells. Pflugers Arch 2002;444:43–51.